A Statically Balanced Compliant Ortho-Planar Mechanism for Low-Frequency Energy Harvesting

Blad, T. W.A.; Van Ostayen, R. A.J.; Herder, J. L.; Tolou, N.

DOI
10.1115/1.4053280

Publication date
2022

Document Version
Final published version

Published in
Journal of Mechanical Design, Transactions of the ASME

T.W.A. Blad[1]
Department of Precision and Microsystems Engineering,
Delft University of Technology,
Delft 2628 CD, The Netherlands
e-mail: t.w.a.blad@tudelft.nl

R.A.J. van Ostayen
Department of Precision and Microsystems Engineering,
Delft University of Technology,
Delft 2628 CD, The Netherlands
e-mail: r.a.j.vanostayen@tudelft.nl

J.L. Herder
Department of Precision and Microsystems Engineering,
Delft University of Technology,
Delft 2628 CD, The Netherlands
e-mail: j.l.herder@tudelft.nl

N. Tolou
Department of Precision and Microsystems Engineering,
Delft University of Technology,
Delft 2628 CD, The Netherlands
e-mail: n.tolou@flexous.com

A Statically Balanced Compliant Ortho-Planar Mechanism for Low-Frequency Energy Harvesting

The usually high eigenfrequencies of miniaturized oscillators can be significantly lowered by reducing the stiffness through stiffness compensation. In this work, a mechanical design for a compliant ortho-planar mechanism is proposed in which the stiffness is compensated to such a degree that it can be identified as statically balanced. The mechanism was fabricated using laser micro-machining and subsequently preloaded through packaging. The statically balanced property of the mechanism was experimentally validated by a measurement of the force–deflection relation. A piezoelectric version of the design was fabricated for the purpose of energy harvesting from low-frequency motion. For a sub 1 Hz excitation, the device demonstrated an average power output of 21.7 μW and an efficiency that compares favorably to piezoelectric energy harvesters reported in the literature. Therefore, it was found that stiffness compensation is a promising method for the design of piezoelectric energy harvesters for low-frequency motions. [DOI: 10.1115/1.4053280]

Keywords: compliant mechanisms, ortho-planar mechanisms, piezoelectric energy harvesting, buckling

1 Introduction

In the last decades, vibration energy harvesting research has led to the development of increasingly smaller devices that scavenge energy from ambient vibration sources, such as human motion. As one of the most promising transduction mechanisms for energy harvesting, the piezoelectric effect has attracted great interest when combined with compliant mechanisms, a field in which mechanisms are synthesized from deforming members. A disadvantage of the desired miniaturization in this context is that the mass scales down at an increased rate compared to the stiffness which leads to higher natural frequencies. Especially for energy harvesting applications, in which the frequencies of ambient motions are generally low, this can greatly reduce the performance [1]. In order to overcome this problem, a negative stiffness element can be employed as a balancer that counteracts the (positive) stiffness of the mechanism [2]. As a result, mechanisms can be obtained that demonstrate near-zero stiffness behavior over a part of their working range [3]. These mechanisms are identified as stiffness-compensated or statically balanced mechanisms. This was demonstrated by Ref. [4], where a statically balanced compliant mechanism (SB-CM) was developed and studied. This mechanism was fabricated using deep reactive-ion etching and achieved a near-zero stiffness characteristic over a small range of motion. In Ref. [5], another SB-CM was demonstrated in which the preloading was induced by thin-film process that is compatible with the fabrication methods used in micro-electromechanical systems (MEMS). The resulting mechanism combined the positive stiffness of a linear guidance mechanism with a post-buckled flexure to achieve static balancing. An oscillator application was shown by Ref. [6] where a MEMS gravimeter is demonstrated that features a proof mass on top of an anti-spring mechanism. With increasing displacement, the anti-spring softened and the system was able to reach a resonant frequency of 2.3 Hz in the vertical orientation. Although low-frequency and bistable systems have been shown for piezoelectric energy harvesting [7,8], the application of SB-CMs to compensate for the stiffness of a piezoelectric transducer has not been demonstrated yet. One explanation may be found in the mismatch between the degrees-of-freedom (DoFs) of most SB-CMs, that move in-plane, and the most widely used piezoelectric transducers for energy harvesting, which are cantilevers that move out of plane. The research objective of this work is to develop a statically balanced compliant ortho-planar mechanism (SB-COM) in which a piezoelectric transducer can be integrated for low-frequency vibration energy harvesting. Moreover, due to its planar design, such a mechanism is compatible with the planar microfabrication processes and therefore allows for miniaturization to micro-scale. In Sec. 2, the mechanical design and method for tuning the stiffness of mechanisms are introduced. Furthermore, the fabrication of the prototypes and experimental methods are discussed. The results are shown and discussed in Sec. 3, and the conclusions are listed in Sec. 4.

2 Methods

2.1 Mechanical Design. Figures 1(*a*) and 1(*b*) show a schematic view of the proposed design of the SB-COM. The design consists of a cantilevered beam, with a length L_c and rigidity EI_c which is connected to a rigid and square shuttle with dimensions of L_m. Two flexures with lengths L_f and rigidities EI_f are connected to the shuttle at right angles to the cantilever. The initially flat flexures can be buckled by compressing them over a distance of dL. This process is called preloading and results in the flexures assuming a post-buckled shape that extends out of plane. In this preloaded configuration, the restoring force delivered by the flexures on the shuttle in the out-of-plane direction is shown in Fig. 1(*c*)(*i*). This force–deflection relation has a negative slope (i.e., stiffness) that is approximately constant over a part of the range of motion [9]. The flexures can be designed using the method outlined in

[1]Corresponding author.

Contributed by the Design Engineering Division of ASME for publication in the Journal of Mechanical Design. Manuscript received May 28, 2021; final manuscript received August 16, 2021; published online February 15, 2022. Assoc. Editor: Massimo Callegari.

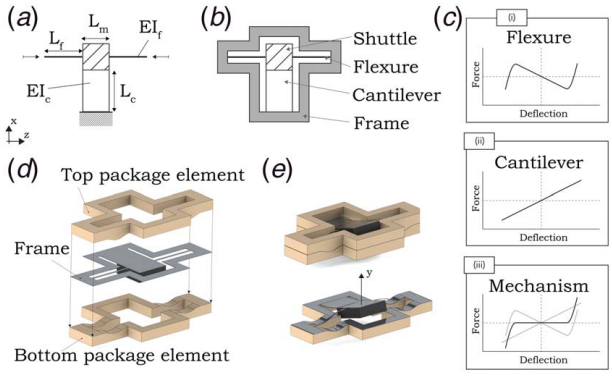

Fig. 1 Design of the proposed SB-COM: (*a*) schematic showing the design parameters; (*b*) schematic overview of the components; (*c*) force–deflection relations of the (*i*) preloaded flexures, (*ii*) cantilever and (*iii*) statically balanced mechanism; (*d*) demonstration of the PIP method; and (e) the assembled structure with and without the top package element

Sec. 2.2, such that this slope is equal and opposite to the restoring force provided by the cantilever (Fig. 1(*c*)(*ii*)). As a result, a statically balanced system can be obtained in which the shuttle is in a state of neutral equilibrium over a part of its range of motion (Fig. 1(*c*)(*iii*)). The method used for preloading the flexures is demonstrated in Figs. 1(*d*) and 1(*e*). In this method, a frame is designed around the mechanism which is sandwiched between two package elements with complementary out-of-plane geometries. As a result, the frame is forced to follow the out-of-plane shape of the packaging elements and therefore shortening it in the in-plane direction to achieve the desired preloading. This method is called package-induced preloading (PIP) and is based on the technique proposed in Ref. [10].

2.2 Stiffness Design Method. To tune the negative slope of the force–deflection relation of the preloaded flexures, the length, L_f, and the flexural rigidity, EI_f, can be manipulated. Compared to the length, tuning the rigidity does not affect the kinematics of the mechanism and is therefore preferred. The rigidity is most conveniently manipulated through the design of the width of the flexures, w_f, as this relation is linear compared to the cubic dependency on the thickness. Moreover, the width is easily controllable with planar manufacturing processes such as laser cutting. Therefore, w_f is chosen as the design parameter to tune the stiffness of the preloaded flexures. In order to determine the configuration for which the desired effect is achieved, a linear buckling analysis is carried out using the finite element model (FEM) described in Sec. 2.4 to identify the buckling modes of the mechanism. From this analysis, the two buckling modes shown in Fig. 2 are found and identified as the modes "W" and "V". The out-of-plane motion of the shuttle can be described as a combination of these modes such that the mechanism moves from mode "W" to mode "V" when the shuttle is displaced away from $y = 0$. It was found that a post-buckled beam can be statically balanced over a particular motion if the critical loads corresponding to the buckling modes that describe this motion are equalized [11]. This principle can also be applied to this mechanism, such that static balancing of the shuttle in the out-of-plane direction is achieved if the critical loads corresponding to the "W" and "V" modes are equal. Finding an optimized value for w_f is done as follows. First, the analytical model presented in Sec. 2.3 is evaluated for a range of values for w_f to find the critical loads of the mechanism. These critical loads depend differently on w_f and values can be found for w_f for which two critical loads are equal. Next, the FEM is used to identify the mode shapes corresponding to these critical loads and fine-tune the value for w_f for which the critical loads of modes "W" and "V" are equal. Finally, the nonlinear force–deflection relation of the post-buckled mechanism is simulated to verify that the resulting configuration is indeed statically balanced.

2.3 Analytical Model. For a beam element with a rigidity, EI, the transverse displacement, y, as a function of the axial coordinate, z corresponding to an applied axial load, P, is governed by the following differential equation [12].

$$\frac{d^4y}{dz^4} + \frac{P}{EI}\frac{d^2y}{dz^2} = 0 \tag{1}$$

The buckling problem of the SB-COM can be formulated as shown in Fig. 3 where the flexures are modeled as two beam elements connecting to a rigid shuttle. Along the length of the flexures, the following points can be identified as the edges of the beam elements: $z_0 = 0$, $z_1 = L_f$, $z_2 = L_f + L_m$, and $z_3 = 2L_f + L_m$. The transverse displacement is therefore given by the following expression:

$$y(z) = u_i(z), \quad z_{2i-2} \le z \le z_{2i-1} \text{ for } i = 1, 2 \tag{2}$$

where u_i is the transverse displacement of the ith flexure. The general solution to Eq. (1) can therefore be found as a piecewise equation with the following form:

$$u_i(z) = A_i \sin\left(\frac{\Lambda}{\sqrt{EI_f}}\, z\right) + B_i \cos\left(\frac{\Lambda}{\sqrt{EI_f}}\, z\right) + C_i z + D_i, \quad \times z_{2i-2} \le z \le z_{2i-1} \text{ for } i = 1, 2 \tag{3}$$

where A_i, B_i, C_i, and D_i are unknown constants that depend on the boundary conditions of the beams and Λ are the eigenvalues

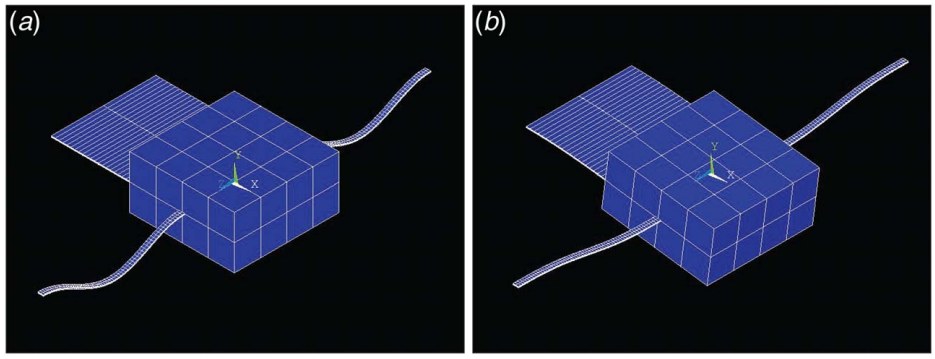

Fig. 2 Finite element model representation of the buckling modes that contribute to the out-of-plane displacement of the shuttle; the modes are identified as (*a*) mode "W" and (*b*) mode "V"

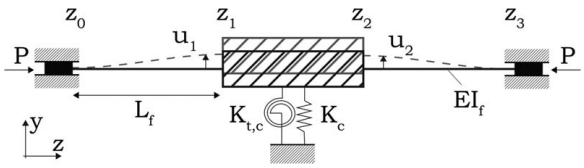

Fig. 3 Schematic of the buckling problem formulated for the SB-COM

corresponding to the critical loads of mechanism such that $\Lambda^2 = P_{crit}$. The boundary conditions that are considered for this mechanism are given by the following equations.

$$y(z_0) = 0 \tag{4.1}$$

$$y(z_3) = 0 \tag{4.2}$$

$$\frac{dy}{dz}(z_0) = 0 \tag{4.3}$$

$$\frac{dy}{dz}(z_3) = 0 \tag{4.4}$$

$$y(z_1) = y(z_2) + L_m \frac{dy}{dz}(z_1) \tag{4.5}$$

$$\frac{dy}{dz}(z_1) = \frac{dy}{dz}(z_2) \tag{4.6}$$

$$\frac{d^2y}{dz^2}(z_1) + K_{t,c}\frac{dy}{dz} = \frac{d^2y}{dz^2}(z_2) \tag{4.7}$$

$$\frac{d^3y}{dz^3}(z_1) - K_c y = \frac{d^3y}{dz^3}(z_2) \tag{4.8}$$

At the outer edges, the beams are fixed in transverse translation and rotation resulting in the boundary conditions as provided by Eqs. (4.1)–(4.4). At the middle connections to the shuttle, continuity is enforced through the boundary conditions given by Eqs. (4.5) and (4.6). Because the shuttle is assumed rigid, the rotations at the points where flexures connect to the shuttle (i.e., z_1 and z_2) must be equal and the transverse displacements at these points can only be offset as a result of the rotation of the shuttle. Finally, Eqs. (4.7) and (4.8) enforce equilibrium in the bending moments and lateral forces. In these equations, terms are included to cover the force and moment exerted by the cantilever as a result of its translational stiffness in the y-direction, K_c, and its torsional stiffness around the x-axis, $K_{t,c}$. These stiffnesses can be found from the following equations where GJ_c is the torsional rigidity of the cantilever

$$K_c = \frac{3EI_c}{\left(L_c + \frac{L_m}{2}\right)^3 - \left(\frac{L_m}{2}\right)^3} \tag{5.1}$$

$$K_{t,c} = \frac{GJ_c}{L_c} \tag{5.2}$$

By applying the boundary conditions given by Eqs. (4.1)–(4.8) to (3), we can find a transcendental eigenvalue problem of the following form [13]:

$$\mathbf{T}(\Lambda)\mathbf{z} = 0 \tag{6}$$

where $\mathbf{T}$ is a matrix consisting of transcendental functions in Λ, and $\mathbf{z}$ is a constant eigenvector containing A_i, B_i, C_i, D_i. The critical loads of the beam are found from the non-trivial solutions of Λ for $\mathbf{z} \neq 0$, and the mode shapes can be found by substituting the result in Eq. (3).

2.3 Finite Element Model. To validate the critical loads found in the analytical model and simulate the force–deflection relation of the mechanisms, FEM was built in ANSYS Mechanical APDL using beam elements (beam188). A linear elastic material model with the properties of spring steel ($E = 190$ GPa, $v = 0.34$, and $\rho = 7.82$ g/cm^3) is used. The buckling modes and their corresponding critical loads are computed by a linear buckling analysis. This analysis is done through eigenvalue buckling in a static structural analysis in which forces were applied to the outer edges of the flexures as shown in Fig. 3. The results from this analysis are used to iteratively fine-tune the optimized value of w_f that was found with the analytical model. The simulation of the force–deflection relation of the post-buckled mechanism was carried out in two steps. First, a preloading step was applied in which the outer edges are displaced inward by a preload displacement dL. Small imperfections were incorporated in the flexures to prevent the simulation from crashing during this step as a result of singularities. After the buckled shape was achieved, the post-buckled mechanism was manipulated in the out-of-plane direction. The reaction forces

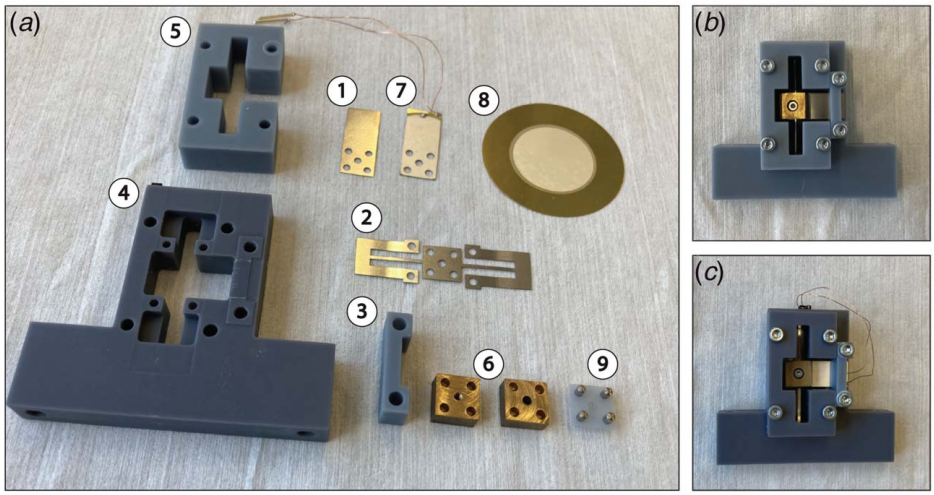

Fig. 4 (*a*) Overview of components and assembled prototypes of the (*b*) SB-COM and (c) SCOPE

Table 1 Relevant parameters of the fabricated prototypes

Parameter	Symbol	Value
SB-COM and SCOPE		
Cantilever length (mm)	L_c	7.5
Cantilever width (mm)	w_c	10
Shuttle length and width (mm)	L_m	10
Preload displacement (mm)	dL	0.2
Flexure length (mm)	L_f	13.5
Thickness of flexures (mm)	t	0.1
Mass of shuttle (g)	m	8
SB-COM		
Cantilever thickness (mm)	t_c	0.1
Flexure width (mm)	w_f	0.52
SCOPE		
Piezoelectric cantilever thickness (mm)	t_p	0.23
Flexure width (mm)	$w_{f,SCOPE}$	0.92

were captured over the range of motion at regular intervals to determine the force–deflection behavior.

2.4 Fabrication and Assembly. To validate the proposed SB-COM design, the components and prototypes shown in Figs. 4(*a*)–4(*c*) were fabricated. The cantilever (1) and flexures (2) are fabricated from 0.1 mm thick spring steel using a Spectra-Physics Talon 355-15 diode-pumped solid-state (DPSS) ultraviolet (UV) laser system with a wavelength of 355 nm and a maximum power of 15 watts at 50 kHz. The cover of the cantilever (3) and the packaging elements (4,5) was three-dimensional (3D) printed from UV photosensitive resin using a PRUSA SL1 and the shuttle (6) was machined from brass. The total mass of the shuttle was 8 g. The elements were aligned by 2×5 mm dowel pins that were inserted in holes in the bottom package element (4) and the bottom half of the shuttle and lined up with holes in the flexure, cantilever, top package element (5) and the top half of the shuttle. The system was assembled by pushing the packaging elements together and clamping them with bolts resulting in the assembled SB-COM shown in Fig. 3(*b*). To evaluate the performance of the design for the application of energy harvesting from low-frequency vibrations, a piezoelectric version of the SB-COM shown in Fig. 3(*c*) was fabricated. This prototype is identified as the SCOPE (i.e., statically balanced compliant ortho-planar piezoelectric energy harvester). In the SCOPE, the stainless steel cantilever is replaced by a piezoelectric transducer (7) with an identical length and width as the cantilever. The transducer was fabricated from $t_p = 0.23$ mm thick audio buzzers (8) (KEPO FT-41T-1.0A1-478) using the laser. The buzzers consisted of a brass substrate with a thickness of 0.1 mm and a piezoelectric layer with a thickness of 0.13 mm to which electrical connections were soldered. To prevent short-circuiting the piezoelectric transducer, a 3D printed isolation layer (9) was added between the transducer and the top of the shuttle. In the SCOPE, the width of the flexures was increased to $w_{f,SCOPE} = 0.92$ mm to compensate for the higher stiffness of the piezoelectric transducer. An overview of the important parameters of both prototypes is given in Table 1.

2.5 Experimental Characterization. The force–deflection relation of the SB-COM was evaluated experimentally with the setup shown in Fig. 5(*a*)(*i*). The setup consists of a force sensor (1) (FUTEK LRM200) mounted on a motorized stage (2) (PI M-505) and connected to the prototype (3). The mechanism is actuated in a quasi-static fashion over a specified range of motion during which the reaction force is captured. The applied deflection is measured by capturing position data from the internal encoder of the stage. Data were recorded with a data acquisition system (4) (NI USB-6008) with a resolution of 50 μm. The connection between the force sensor and the prototype shown in Fig. 5(*a*)(*ii*) is made by using a magnet that latches onto the bolt in the middle of the shuttle. This ensures that the force sensor remains in contact with the prototype such that also pulling forces can be measured. The energy harvesting performance of the SCOPE was evaluated by

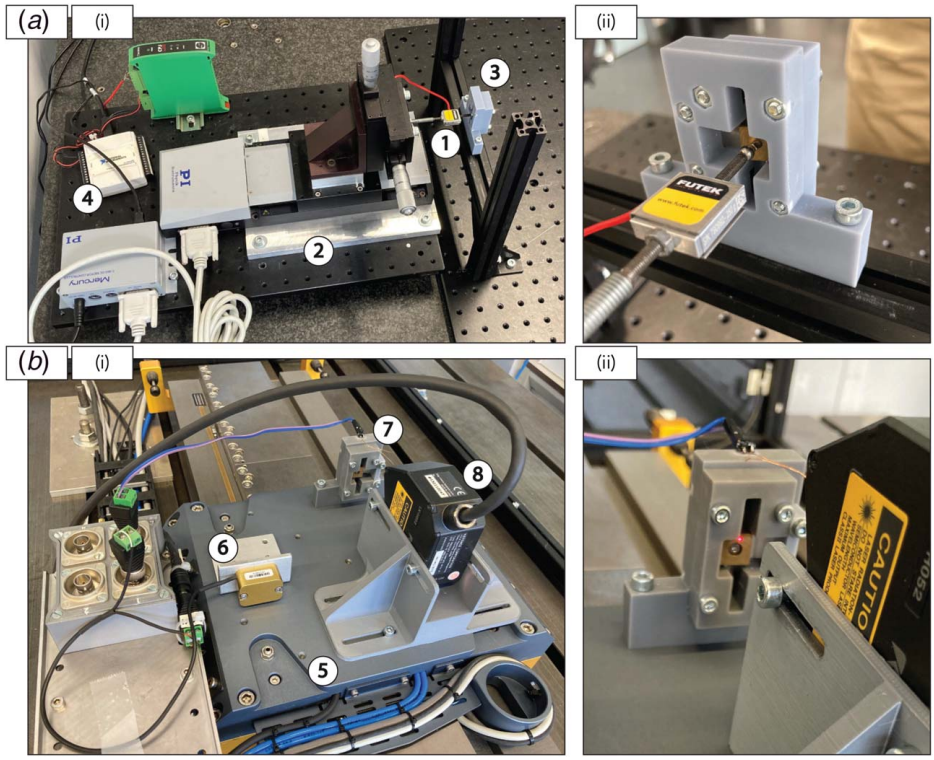

Fig. 5 Experimental setups used for (*a*) the validation of the force–deflection relation of the SB-COM and (*b*) measuring the performance of the SCOPE under low-frequency vibration

using the setup shown in Fig. 5(*b*)(*i*) to apply a prescribed motion to the package. The setup consists of a platform (5) suspended by air bearings that can be moved over a distance of 500 mm. The platform is driven by an ironless linear motor (TECNOTION UL-6N) controlled by a servo drive (KOLLMORGEN AKD-P00306). The position of the platform is measured using an incremental encoder (RENISHAW TONIC T1000-05A) and controlled using a position feedback loop. Moreover, the acceleration of the platform was also captured using an accelerometer (6) (ME-MEßSYSTEME AS28E). The prototype (7) was fastened on top of the platform in an orientation such that the motion is applied in the *y*-direction and the and the displacement of the shuttle was captured using a laser sensor (8) (KEYENCE LS-K052) as shown in Fig. 5(*b*)(*ii*). The power output of the piezoelectric transducer was measured over a 100 KΩ load.

3 Results and Discussion

3.1 Mechanical Analysis. The first three buckling modes of the SB-COM and their corresponding critical loads are shown in Fig. 6. In this figure, the dashed lines are obtained with the analytical model and the solid lines are obtained with the linear buckling analysis carried out using the FEM. It can be found that next to the "W" and "V" modes also another mode is found that can be identified as the "N" mode. This mode describes a rotation of the shuttle is therefore not relevant for achieving a configuration in which the shuttle is statically balanced in the out-of-plane direction. It can be observed that manipulating the design variable w_f has a different effect on the critical loads corresponding to these modes and that the order of the buckling mode changes over the considered region. As discussed in Sec. 2.2, the desired near-zero stiffness is achieved if the critical loads corresponding to the "W" and "V" modes are equalized because these modes describe the out-of-plane displacement. It can be found from the figure that this effect is achieved in the SB-COM at a flexure width of $w_f = 0.52$ mm. Following a similar analysis, this effect was found for the SCOPE at a flexure width of $w_{f,SCOPE} = 0.92$ mm. It can be seen that the analytical model presented in Sec. 2.3 provides a relatively good estimate of the critical loads calculated by the FEM. This is an important result as this analytical model can be evaluated much quicker. While the critical load of the "W" mode overlaps completely with the value calculated by the FEM, slight differences can be found in the values calculated for the "V" and "N" modes. These differences are most likely a result of the simplified representation of the displacement of the mechanism; in the analytical model, the displacement is assumed to be a translation in the out-of-plane direction, while in reality, the proof mass will undergo a pivoting motion around the base of the cantilever.

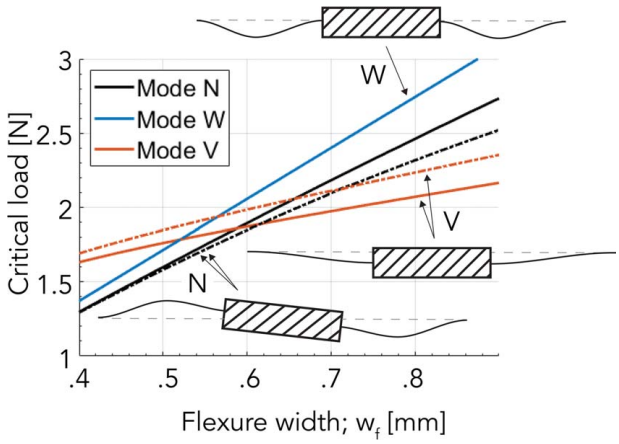

Fig. 6 Buckling modes and corresponding critical loads as a function of the design variable w_f for the SB-COM; (dashed) analytical model, (solid) finite element model

3.2 Force–Deflection Relation of the SB-COM. The measured force–deflection relations of SB-COM with and without flexures are compared to the results of the simulations in Figs. 7(*a*) and 7(*b*). From the results of the simulation shown in Fig. 7(*a*) can be verified that without the flexures, the stiffness of the cantilever is 265 N/m and corresponds to the stiffness that can be calculated from Eq. (5.1). Furthermore, it can be observed from the simulation shown in Fig. 7(*b*) that a much flatter force–deflection relation is found for the SB-COM when the flexures with a width of $w_f =$ 0.52 mm were added. In this configuration, the shuttle demonstrates a region of near-zero stiffness and virtually no force when deflected between approximately $y = -2$ mm and $y = 2$ mm. Therefore, this configuration can be identified as statically balanced. Moreover, it can be observed the force–deflection relation rapidly steepens for displacements of $|y| > 2$ mm. This steepening effect is a result of the flexures being straightened such that they lose their compensating effect and are loaded in tension instead.

The measured force–deflection relations contain a hysteresis between the forward and backward load paths which is caused by the magnetic connection between the shuttle and the force sensor. Overall, they show a good correspondence to the simulated results. It can be seen that the greatest differences are observed in the near-zero stiffness region of the SB-COM with flexures $y =$ 0 mm and $y = 2$ mm. These differences are mainly a result of manufacturing tolerances and the manual assembly that resulted in a slight preference of the mechanism to one of the sides.

3.3 Energy Harvesting With the Scope. The results of the low-frequency energy harvesting experiment of SCOPE with and without flexure are shown in Figs. 8(*a*) and 8(*b*). In this experiment, the platform is moved with a harmonic motion with a frequency of 0.9 Hz and an amplitude of 230 mm such that an acceleration of 0.75 g is applied to the SCOPE. It can be seen from the figures that energy harvesting is demonstrated for this low-frequency excitation of sub 1 Hz.

From the figure can be seen that while the SCOPE without flexures demonstrates performance that is typical for linear oscillators at off-resonance conditions, the SCOPE with flexures was very lightly bistable and demonstrates a motion pattern where the shuttle rapidly moves through the low stiffness zone until it encounters an increase in the restoring force. The asymmetry in this motion pattern can likely be explained due to a slight preference of the mechanism resulting from the manufacturing tolerances and manual assembly. Moreover, at the displacement of $y = -2$, this leads to an impact-like behavior, presumably due to the rapid steepening of the force–deflection relation at this point, which greatly improves the power output of the piezoelectric transducer. Moreover, the average power dissipated in the resistor over the 5-s interval shown in Figs. 8(*a*) and 8(*b*) is 0.1 μW for the SCOPE without flexures and 21.7 μW for the SCOPE with flexures. The experiment is repeated for excitations of 1, 3, 5, 7, and 9 Hz for accelerations of 0.5 and 1 g, and the resulting frequency–power curves are shown in Figs. 9(*a*) and 9(*b*). From Fig. 9(*b*), it can be observed that the SCOPE with flexures demonstrated a very high power output for accelerations of 1 g at all frequencies, but demonstrated virtually no power output for accelerations of 0.5 g. This result can be explained by the observed bistability of the SCOPE with flexures. Although the device was only very lightly bistable, the acceleration of 0.5 g was not sufficient to provide enough force to set the shuttle in motion.

3.4 Efficiency of the SCOPE. To compare the performance of the SCOPE with piezoelectric energy harvesters reported in literature, the motion ratio, λ, and generator figure of merit, FoM_G, are used [14]. The motion ratio is a metric to describe the size of the generator relative to the applied excitation and the FoM_G is a metric with which a bias-free comparison can be drawn between generators of different shapes and sizes operated at different

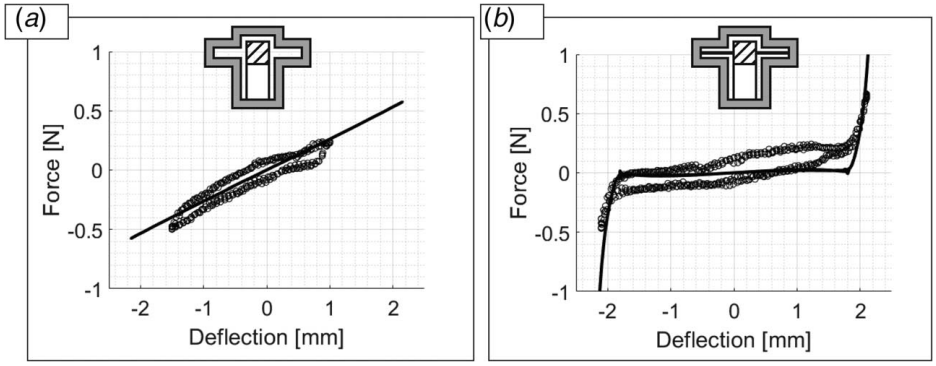

Fig. 7 Measurement and simulation of the force–deflection relations of the SB-COM (*a*) without flexures and (*b*) with flexures; — FEM, o measurement

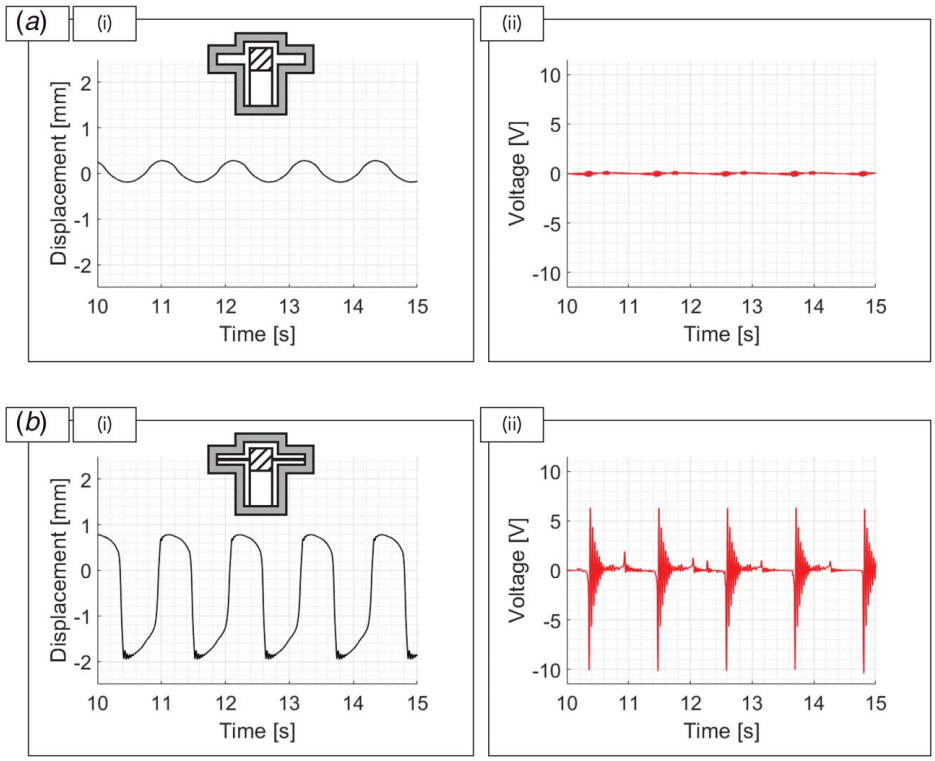

Fig. 8 Measured (*i*) displacement and (*ii*) voltage over a 100-KΩ resistor when excited by a harmonic motion with a frequency of 0.9 Hz and an acceleration of 0.75 g for the SCOPE (*a*) without flexures and (*b*) with flexures

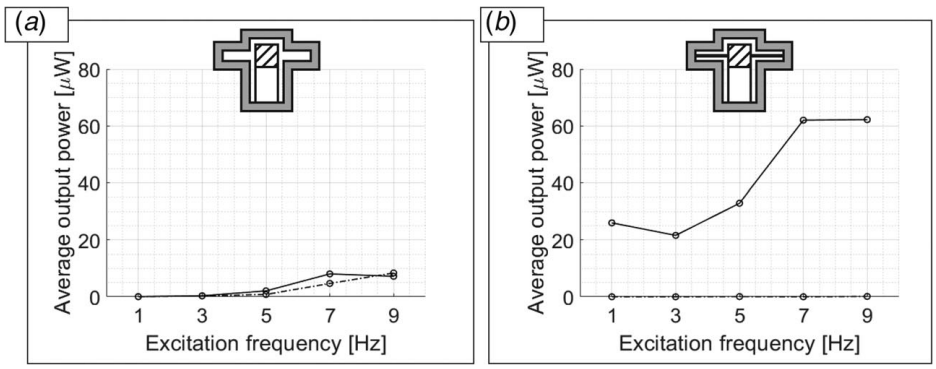

Fig. 9 Frequency–power curves of the SCOPE (*a*) without flexures and (*b*) with flexures at accelerations of (dashed) 0.5 g, and (solid) 1 g

Table 2 Performance of the SCOPE compared to piezoelectric energy harvesters reported in literature

Source	Driving motion	Output power (μW)	Motion ratio	Efficiency
This work	0.9 Hz, 0.75 g	21.7	0.033	0.27%
[15]	2 Hz, 2 g	10.4	0.057	0.13%
[16]	1 Hz, 1 g	47	0.070	0.18%
[17]	0.25 Hz, 0.28 g	370	0.063	1.00%

conditions. These quantities are defined by the following expressions:

$$\lambda = \frac{L_z}{2Y_0} \tag{7.1}$$

$$FoM_G = \frac{P_{avg}}{\frac{1}{16} Y_0 \rho_m V L_z \omega^3} \times 100\% \tag{7.2}$$

where Y_0 and ω are the amplitude and frequency of the driving motion, V is the total volume occupied by the device, L_z is the dimension of the generator along the direction of the applied motion, ρ_m is the density of the proof mass material, and P_{avg} is the average output power dissipated in the resistive load. For the SCOPE with flexures, which has a dimension of $L_z = 15$ mm, a motion ratio of $\lambda = 0.033$ is found for the sub 1 Hz excitation with an amplitude of 230 mm. This constitutes one of the lowest motion ratios reported in literature yet and demonstrates that this energy harvester is tested under conditions representative of a very high level of miniaturization [14]. Moreover, efficiency of 0.27% was found at an average power output of 21.7 μW for the $50 \times 32 \times 15$ mm device. In Table 2 these results are compared to other devices reported in literature and it can be found that the SCOPE demonstrates a relevant efficiency for an energy harvester at such a low motion ratio. Furthermore, it is expected that higher efficiencies can be achieved when a larger transducer is used in which more piezoelectric material is deformed and when the used volume is further optimized.

Conclusion

In this work, we have demonstrated a new ortho-planar mechanism design consisting of a cantilever and two post-buckled flexures mounted at right angles. The out-of-plane stiffness of the mechanism can be tuned by manipulating the width of the flexures. Moreover, it was demonstrated that a statically balanced configuration could be achieved by tuning the width of the balancing flexures to 0.52 mm. The mechanism was prototyped using laser micromachining and subsequently preloaded using a packaging method called package-induced preloading. The statically balanced property of the mechanism was experimentally validated by a measurement of the force–deflection relation. Furthermore, a piezoelectric energy harvester prototype is fabricated by replacing the cantilever of the mechanism with a piezoelectric transducer. The power output of the energy harvester is evaluated at a low-frequency excitation of sub 1 Hz using a linear stage. Under these conditions, the statically balanced energy harvester demonstrates a relevant efficiency and greatly improved performance compared to a configuration in which the flexures were removed. Therefore, it can be concluded that static balancing can be used to improve the performance of piezoelectric energy harvesters for low-frequency vibrations.

Conflict of Interest

There are no conflicts of interest.

Data Availability Statement

The data sets generated and supporting the findings of this article are obtainable from the corresponding author upon reasonable request. The authors attest that all data for this study are included in the paper.

References

[1] Roundy, S., 2005, "On the Effectiveness of Vibration-Based Energy Harvesting," J. Intell. Mater. Syst. Struct., **16**(10), pp. 809–823.

[2] Schenk, M., and Guest, S. D., 2014, "On Zero Stiffness," Proc. Inst. Mech. Eng. Part C J. Mech. Eng. Sci., **228**(10), pp. 1701–1714.

[3] Hoetmer, K., Herder, J. L., and Kim, C. J., 2010, "A Building Block Approach for the Design of Statically Balanced Compliant Mechanisms," ASME 2009 International Design Engineering Technical Conferences and Computers and Information in Engineering Conference, San Diego, CA, Aug. 30–Sept. 2, pp. 313–323.

[4] Tolou, N., Estevez, P., and Herder, J. L., 2012, "Collinear-Type Statically Balanced Compliant Micro Mechanism (SB-CMM): Experimental Comparison Between Pre-Curved and Straight Beams," ASME 2011 International Design Engineering Technical Conferences and Computers and Information in Engineering Conference, Washington, DC, Aug. 28–31, pp. 113–117.

[5] Kuppens, P. R., Herder, J. L., and Tolou, N., 2019, "Permanent Stiffness Reduction by Thermal Oxidation of Silicon," J. Microelectromech. Syst., **28**(5), pp. 900–909.

[6] Middlemiss, R. P., Samarelli, A., Paul, D. J., Hough, J., Rowan, S., and Hammond, G. D., 2016, "Measurement of the Earth Tides With a MEMS Gravimeter," Nature, **531**(7596), pp. 614–617.

[7] Abdelkefi, A., Barsallo, N., Tang, L., Yang, Y., and Hajj, M. R., 2014, "Modeling, Validation, and Performance of Low-Frequency Piezoelectric Energy Harvesters," J. Intell. Mater. Syst. Struct., **25**(12), pp. 1429–1444.

[8] Liu, W., Badel, A., Formosa, F., Wu, Y., Bencheikh, N., and Agbossou, A., 2015, "A Wideband Integrated Piezoelectric Bistable Generator: Experimental Performance Evaluation and Potential for Real Environmental Vibrations," J. Intell. Mater. Syst. Struct., **26**(7), pp. 872–877.

[9] Howell, L. L., 2013, "Compliant Mechanisms," *Proceedings of the 21st Century Kinematics*, J. M. McCarthy, ed., Springer, London, pp. 189–216.

[10] Mariello, M., Blad, T. W. A., Mastronardi, V. M., Madaro, F., Guido, F., Staufer, U., Tolou, N., and De Vittorio, M., 2021, "Flexible Piezoelectric AlN Transducers Buckled Through Package-Induced Preloading for Mechanical Energy Harvesting," Nano Energy, **85**(1), p. 105986.

[11] Blad, T. W. A., van Ostayen, R. A. J., and Tolou, N., 2021, "A Method for Tuning the Stiffness of Building Blocks for Statically Balanced Compliant Ortho-planar Mechanisms," Mech. Mach. Theory, **162**(1), p. 104333.

[12] Timoshenko, S. P., and Gere, J. M., 1964, *Theory of Elastic Stability*, McGraw-Hill, New York.

[13] Singh, K. V., and Li, G., 2009, "Buckling of Functionally Graded and Elastically Restrained Non-uniform Columns," Composites, Part B, **40**(5), pp. 393–403.

[14] Blad, T. W. A., and Tolou, N., 2019, "On the Efficiency of Energy Harvesters: A Classification of Dynamics in Miniaturized Generators Under Low-Frequency Excitation," J. Intell. Mater. Syst. Struct., **30**(16), pp. 2436–2446.

[15] Galchev, T., Aktakka, E. E., and Najafi, K., 2012, "A Piezoelectric Parametric Frequency Increased Generator for Harvesting Low-Frequency Vibrations," J. Microelectromech. Syst., **21**(6), pp. 1311–1320.

[16] Renaud, M., Fiorini, P., van Schaijk, R., and Hoof, C., 2009, "van Harvesting Energy From the Motion of Human Limbs: The Design and Analysis of an Impact-Based Piezoelectric Generator," Smart Mater. Struct., **18**(3), p. 035001.

[17] Pillatsch, P., Yeatman, E. M., and Holmes, A. S., 2012, "A Scalable Piezoelectric Impulse-Excited Energy Harvester for Human Body Excitation," Smart Mater. Struct., **21**(11), p. 115018.